CELL BIOLOGY

Transient activation of the UPR^{ER} is an essential step in the acquisition of pluripotency during reprogramming

Milos S. Simic[1,2,3], Erica A. Moehle[1,2,3], Robert T. Schinzel[1,2,3], Franziska K. Lorbeer[3], Jonathan J. Halloran[1,2,3], Kartoosh Heydari[3], Melissa Sanchez[1,2,3], Damien Jullié[4], Dirk Hockemeyer[3], Andrew Dillin[1,2,3]*

Somatic cells can be reprogrammed into pluripotent stem cells using the Yamanaka transcription factors. Reprogramming requires both epigenetic landscape reshaping and global remodeling of cell identity, structure, basic metabolic processes, and organelle form and function. We hypothesize that variable regulation of the proteostasis network and its influence upon the protein-folding environment within cells and their organelles is responsible for the low efficiency and stochasticity of reprogramming. We find that the unfolded protein response of the endoplasmic reticulum (UPR^{ER}), the mitochondrial UPR, and the heat shock response, which ensure proteome quality during stress, are activated during reprogramming. The UPR^{ER} is particularly crucial, and its ectopic, transient activation, genetically or pharmacologically, enhances reprogramming. Last, stochastic activation of the UPR^{ER} predicts reprogramming efficiency in naïve cells. Thus, the low efficiency and stochasticity of cellular reprogramming are due partly to the inability to properly initiate the UPR^{ER} to remodel the ER and its proteome.

INTRODUCTION

Reprogramming of somatic cells into induced pluripotent stem cells (iPSCs) highlights the remarkable plasticity found within cells and provides incredible potential for cell biology and regenerative medicine (*1*). Cellular reprogramming can be achieved by the forced expression of OCT4, SOX2, KLF4, and c-MYC, transcription factors with a wide range of target genes (*2*). However, the success of cellular reprogramming of human cells is extremely low, ranging from .0001 to .1%. The mechanisms that drive the variability and stochastic nature of reprogramming are enigmatic and pose one of the major hurdles in the reprogramming process (*3*, *4*). Therefore, a better understanding of the mechanisms underlying reprogramming is necessary to improve this process (*5*).

It is clear that genome integrity and epigenetic rewiring are central tenets of the reprogramming process and could explain much of the variation within the acquisition of the pluripotent state. However, as the somatic cell transitions into a new identity with changes in epigenetic wiring, the constituents and quality of its subcellular organelles are also undergoing massive rewiring and are under selective pressure to ensure a pristine proteome of the resulting immortal iPSC. Inheritance of faulty proteins and organelles provides challenges upon a cell driving toward immortality and pluripotency. Therefore, the stress during this process is not only confined within the nucleus but also emanates throughout the cell and subcellular organelles. To ensure a proper balance of proteome function and organelle integrity, a delicate network exists that monitors and responds to challenges within the proteomes of subcellular organelles, known as the proteostasis network. Within the proteostasis network, key stress responses—such as the endoplasmic reticulum unfolded protein response (UPR^{ER}), which monitors the integrity of the endoplasmic reticulum (ER), the mitochondrial unfolded protein response (UPR^{mt}), which monitors mitochondrial quality, and the heat shock response (HSR), which predominantly interrogates the cytoplasm—govern and dictate proteome fidelity and organelle function (*6*).

Secreted and membrane-bound proteins are synthesized in the ER and represent up to one-third of the total proteome produced by cells. Increased protein synthesis, cell differentiation, tissue development, senescence, DNA damage, and many other stressors disrupt ER homeostasis and activate the UPR^{ER} (*7*). Three ER-resident transmembrane proteins sense the protein folding state in the ER lumen and transduce this information using parallel and distinctive signal transduction mechanisms: ATF6 (activating transcription factor 6), PERK (double-stranded RNA-activated protein kinase–like ER kinase), and IRE1 (inositol-requiring enzyme 1) (*7*). During stress, IRE1 converges on the X-box binding protein 1 transcription factor (XBP1), causing its cytoplasmic splicing to create the *XBP1s* mRNA that can be translated and incorporated into the nucleus to regulate hundreds of genes required for ER protein folding and morphology (*8*, *9*). PERK functions to decrease global translation by phosphorylation of eIF2α (*10*) while specifically increasing translation of the transcription factor ATF4 (*11*). Furthermore, ATF6 is shuffled from the ER to the Golgi, where two Golgi-resident proteases cleave it, releasing its cytosolic DNA binding domain that enters the nucleus and activates target genes (*12*).

Cellular reprogramming causes a marked change in cell morphology and promotes the remodeling of many organelles such as mitochondria (*13*). We therefore hypothesized that cellular reprogramming should restructure the ER and require the UPR^{ER}. Furthermore, the UPR^{ER} presents stochastic variation among isogenic cell populations, with some cells mounting a robust response and others feebly attempting induction. We further speculated that the UPR^{ER} might not only play a pivotal role during reprogramming but could also explain its stochastic nature and could predict, at least in part, this inherent stochasticity.

RESULTS

Cellular reprogramming activates the UPR^{ER}, HSR, and UPR^{mt}

During stress, the transcription of central regulators of the proteostasis network is increased, as well as their downstream targets (*6*).

[1]Howard Hughes Medical Institute, University of California, Berkeley, Berkeley, CA 94720, USA. [2]California Institute for Regenerative Medicine, Berkeley, CA 94720, USA. [3]University of California, Berkeley, Berkeley, CA 94720, USA. [4]University of California, San Francisco, San Francisco, CA 94143, USA.
*Corresponding author. Email: dillin@berkeley.edu

We analyzed the canonical downstream transcriptional targets of the UPR^{ER} (HSPA5 and GRP94), HSR (HSPA1A), and UPR^{mt} (GRP75) during reprogramming of neonatal fibroblasts and found that transcriptional targets of each response were increased compared with cells not undergoing reprogramming (Fig. 1A). This observation was extended to reprogramming of neonatal keratinocytes as well (fig. S1A). During the reprogramming process, the four reprogramming factors are delivered by viral infection. To exclude the possibility that the UPR^{ER} is induced by the use of a viral delivery system, we also used an episomal delivery system of the reprogramming factors and found similar activations of the HSR, UPR^{ER}, and UPR^{mt} (fig. S1B). To corroborate the mRNA levels, we analyzed the HSPA5, GRP94, HSPA1A, and GRP75 protein levels and found that they too were increased (Fig. 1B and fig. S1C). The differences in protein levels between green fluorescent protein (GFP) day 3 and GFP day 6 are due to the time at which cells were moved to iPSC reprogramming media on day 4. Therefore, each comparison was normalized to its respective control GFP. The activation of the UPR^{ER} and HSR was similar to what is found in cells undergoing an ER stress (tunicamycin treatment) or a heat shock (42°C incubation), respectively (fig. S1, D and E). We also confirmed by both mRNA and protein levels that overexpression of GFP did not activate the stress pathways (Fig. 1B and fig. S1, F and G).

Because of the important role of the UPR^{ER} in stem cells and during differentiation (*14*), we decided to further characterize its activation during cellular reprogramming. We analyzed the phosphorylated state of IRE1 and PERK, modifications indicative of ER stress, and found that both were highly phosphorylated during the reprogramming process (Fig. 1C and fig. S2A). In all cases, we observed a transient up-regulation of the UPR^{ER} that was not prolonged or extended after the acquisition of pluripotency. The phosphorylation of IRE1 leads to the cytosolic splicing of XBP1 mRNA. Consistent with the activation of IRE1, we observed increased spliced mRNA of XBP1 in both fibroblasts (Fig. 1D) and keratinoyctes undergoing reprogramming (fig. S2B). The mRNA levels of CHOP, a canonical downstream target of the PERK pathway, were also increased in both fibroblasts and keratinoyctes (fig. S2C). Last, we tested the activation of the third branch of the UPR^{ER} pathway, the transcriptional activation of ATF6 (*15*). We found that ATF6 mRNA levels in both fibroblasts and keratinocytes were increased during cellular reprogramming (fig. S2D).

The ER is composed of an orchestrated architecture that can be dynamic to include tubular geometry fused with undulant sheets. By electron microscopic (EM) analysis, the ER, pseudocolored in red, of cells undergoing reprogramming appears largely tubular, lacking sheet structures (Fig. 1E). The network and the high branching aspect seen in control cells are lost during reprogramming. It appears that the volume of the ER is decreased as well. The ER of cells undergoing reprogramming resembles that of cells treated with the ER stressor, tunicamycin (fig. S2E). Molecularly, levels of reticulon 4 (a marker of tubular ER) were increased and CLIMP-63 (a marker of cisternae/sheets) was decreased (*16*) during reprogramming, consistent with the EM analysis, revealing tubular ER structures and few sheet structures (fig. S2A).

Tubular ER morphology is associated with impaired secretory capacity. We tested the secretion capacity of cells undergoing reprogramming by following the secretion of the exogenously expressed humanized Gaussia luciferase protein (Gluc) (*17*). We collected the supernatant of cells undergoing reprogramming and observed a marked reduction in secreted Gluc. The reduced secretion of Gluc during reprogramming was not due to decreased expression of the Gluc transgene during the reprogramming process (Fig. 1F).

Consistent with increased ER stress, morphological remodeling of the ER, and reduced ER secretory function during the reprogramming process, we also found that cells undergoing reprogramming were more resistant to exogenous ER stress than control cells. Using a dose-survival curve for cells grown in the presence of tunicamycin, we found that cells undergoing reprogramming were more protected than cells not attempting to acquire pluripotency (Fig. 1G). In sum, ER stress, morphology, and function are markedly altered during the cellular reprogramming process, and it appears to be transient and not retained in the ensuing pluripotent cell.

Advanced states of reprogramming positively correlate with UPR^{ER} activation

Intrigued by the findings that the ER undergoes profound changes as a cell transitions from a basic, unilateral fate to one that is expansive and pluripotent, we began to query the major driver of ER remodeling and stress to understand what role, if any, did the UPR^{ER} play in cellular reprogramming. To decipher the role of the UPR^{ER} during reprogramming and to test if it could be a limiting factor (i.e., essential) for successful reprogramming, we created somatic cells that contained a visible marker of UPR^{ER} induction. Briefly, we followed the induction of the endogenous UPR^{ER} target gene HSPA5 by fusing enhanced GFP (eGFP) onto its C terminus. Using transcription activator-like effector nuclease (TALENs)–mediated genome editing, we inserted eGFP to the last amino acid of HSPA5 in H9 embryonic stem cells (ESCs) (fig. S3A). Successful targeting was confirmed by Southern blot (Fig. 2A) and Western blot analyses (Fig. 2B) as the predicted HSPA-GFP fusion protein is recognized by both GFP and HSPA5 antibodies. No other GFP-specific bands were observed, suggesting that any potential off-target integrations were not translated. The proper integration was further confirmed by sequencing of the targeted locus (fig. S3A). The HSPA5-GFP cell line was then differentiated into somatic fibroblast-like cells (*18*). The resulting somatic cells were then used for cellular reprogramming to assess how the UPR^{ER} responded during cellular reprograming. As a control for reprogramming experiments, the HSPA5-GFP somatic cells responded faithfully to the ER stress caused by tunicamycin, showing robust GFP fluorescence detectable by fluorescence microscopy, protein levels (Fig. 2B), and fluorescence-activated cell analysis (Fig. 2C). The induction was reversible. After removal of tunicamycin, GFP levels decreased over time in these reporter cells (Fig. 2C), indicating that the reporter faithfully portrayed ER stress induction and not overt cellular damage.

Equipped with a reliable live cell marker for ER stress, we now needed to couple it to molecular signatures of the process of cellular reprogramming (*19*). The process of reprogramming can be followed by the abundance of various cellular proteins located on the plasma membrane. During successful reprogramming, the pluripotency markers, SSEA-4 and TRA-1-60, are progressively enriched on the plasma membrane (*20*). SSEA-4 and TRA-1-60 appear sequentially, with the latter serving as a marker of cells further along the reprogramming process and more likely to provide the rare pluripotent cells (*20*). Therefore, the simultaneous presence of both SSEA-4 and TRA-1-60 is an indication of cells further along in the reprogramming process (Fig. 2, D and I), while cells only positive for

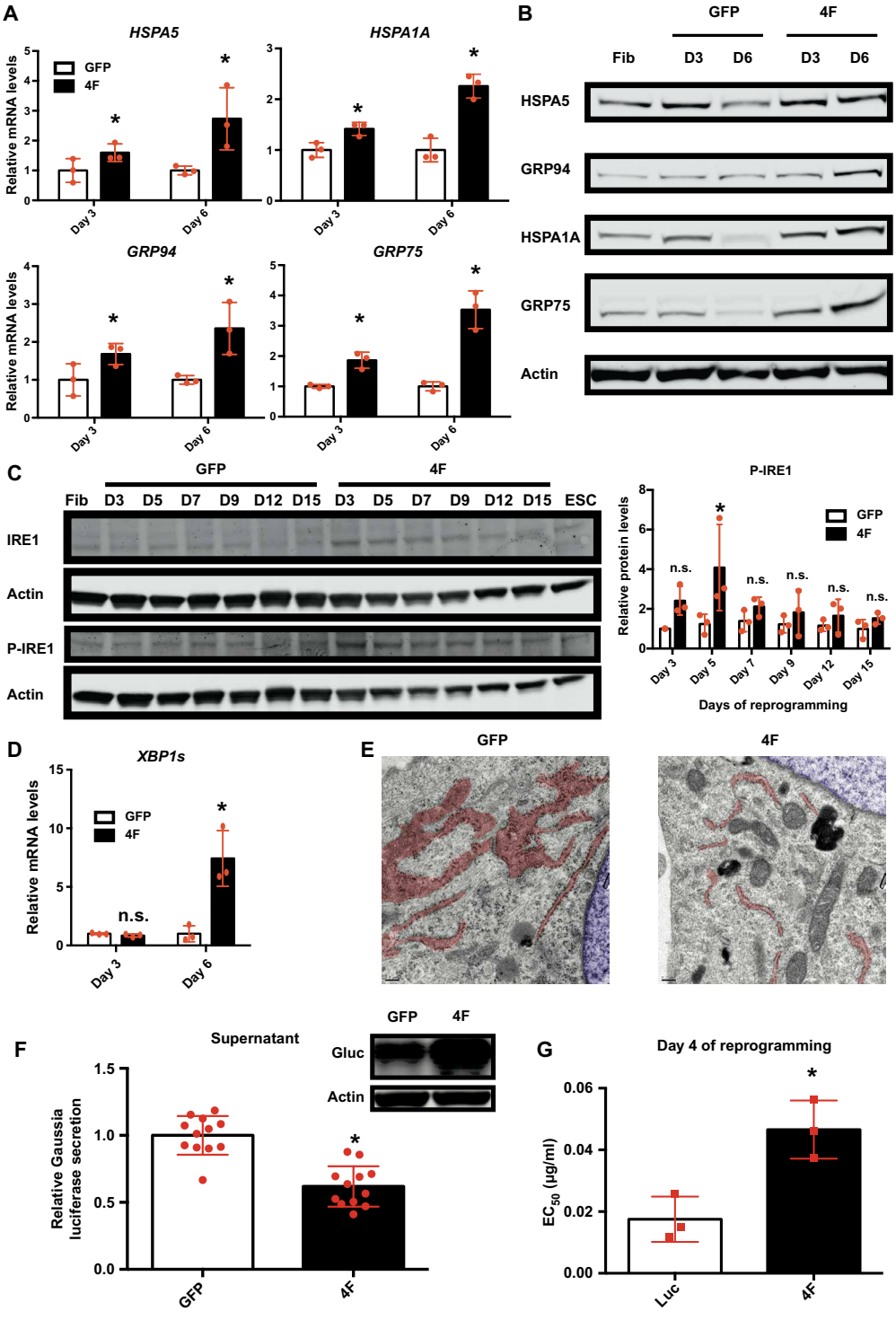

Fig. 1. The three major unfolded protein responses are activated during cellular reprogramming. (**A**) Relative mRNA levels of the main effectors of the UPR^{ER} (HSPA5 and GRP94), HSR (HSPA1A), and UPR^{mt} (GRP75) relative to *GAPDH* determined by quantitative reverse transcription polymerase chain reaction (qRT-PCR) ($n = 3$, average ± SD). GFP control was set to 1 for each day. (**B**) Western blot analysis of the main effectors of the UPR^{ER} (HSPA5 and GRP94), HSR (HSPA1A), and UPR^{mt} (GRP75). D, day. (**C**) Time course reprogramming Western blot analysis of P-IRE1 and IRE1 with P-IRE1 quantification ($n = 3$, average ± SD). *$P < 0.05$, statistical difference using a Sidak multiple comparison test; n.s., statistical nonsignificance. (**D**) Relative mRNA levels of the spliced form of *XBP1* relative to *GAPDH* determined by qRT-PCR ($n = 3$, average ± SD). GFP control was set to 1 for each day. (**E**) Electron microscopy of day 4 reprogramming fibroblasts and GFP control. Scale bar, 0.2 µm. Pseudocolors blue and red mark, respectively, the nucleus and the ER. (**F**) Secretion capability of the ER measured by luciferase activity secreted in the media ($n = 12$, average ± SD) and Western blot analysis of the Gaussia luciferase. (**G**) Sensitivity to tunicamycin treatment determined by median effective concentration (EC_{50}) measurement at day 4 of reprogramming of fibroblast-like cells ($n = 3$, average ± SD). *$P < 0.05$, statistical difference using an unpaired two-tailed *t* test.

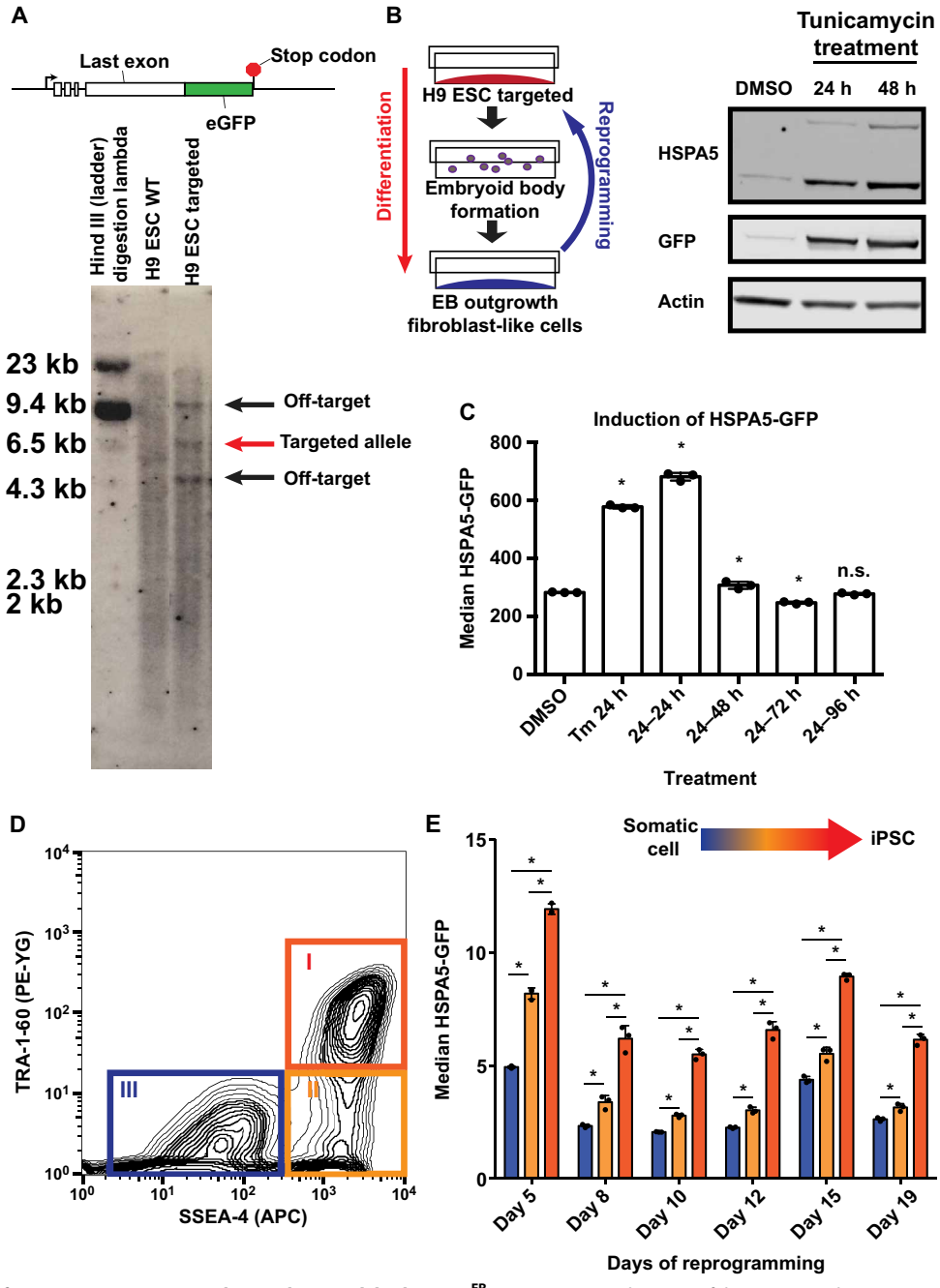

Fig. 2. Advanced state of reprogramming positively correlates with higher UPR^{ER}activation. (**A**) Schematic of the genome editing strategy and Southern blot using a GFP probe. The red arrow shows the expected size of the targeted allele, while the black arrows show two off-target integrations. WT, wild type. (**B**) Schematic of the fibroblast-like cell differentiation protocol (left) and Western blot of HSPA5, GFP, and actin showing the dynamical induction of the reporter line after the addition of tunicamycin (0.1 μg/ml). The predicted HSPA5-GFP fusion band was targeted by both GFP and HSPA5 antibodies using dual-channel imaging with the Odyssey CLx Imaging System confirming the correct targeting. Only a single intense specific GFP band was observed, suggesting that the off-target integrations are not translated (right). (**C**) Median HSPA5-GFP levels analyzed by flow cytometry upon tunicamycin (0.1 μg/ml) treatment for 24 hours and after removal ($n = 3$, average ± SD). *$P < 0.05$, statistical difference using Dunnett's multiple comparison test to the DMSO control. (**D**) Flow cytometry analysis of fibroblast-like HSPA5-GFP cells at day 8 of reprogramming stained with SSEA-4 and TRA-1-60 surface markers. I, II, and III represent the different cell states of reprogramming. (**E**) Median HSPA5-GFP of the different cell states (I, II, and III) during reprogramming ($n = 3$, average ± SD). *$P < 0.05$, statistical difference using Newman-Keuls multiple comparison test between all the conditions.

SSEA-4 and lacking TRA-1-60 would be lagging in the process (Fig. 2D, II). Last, cells with neither of these markers are the furthest from achieving the reprogrammed state (Fig. 2D, III) (*19*, *21*, *22*). On the basis of the distinction of the different reprogramming states using these makers, we analyzed the levels of HSPA5-GFP at different time points of reprogramming to ask if the UPR^{ER} induction correlated with increased reprogramming efficiency. Consistently and robustly, we observed the highest levels of HSPA5-GFP

in the cells that had progressed the furthest in the reprogramming process—the SSEA-4 and TRA-1-60 double-positive cells (Fig. 2E).

To validate the UPR^{ER} GFP reporter, we sorted the three populations (I, II, and III) at day 7 of reprogramming, a time when the UPR^{ER} is normally and transiently induced (Fig. 1C), and measured UPR^{ER} induction levels by mRNA levels of UPR^{ER} target genes (*XBP1s*, *CHOP*, and *GRP94*). As expected, we found the highest level of UPR^{ER} target gene induction in the SSEA-4^{+}/TRA-1-60^{+} cells (I population; fig. S3B). In addition, we confirmed that the SSEA-4^{+}/TRA-1-60^{+} population (I) was the most progressed toward reprogramming by analyzing the reactivation of endogenous pluripotency marker genes (fig. S3C). Together, cells with a more advanced state of reprogramming also contained the highest induction of the UPR^{ER} by multiple measurements, indicating that proficiency of reprogramming is consistent and corollary with UPR^{ER} induction.

Activation of the UPR^{ER} increases reprogramming efficiency

Because of the correlation between increased UPR^{ER} induction and progression toward the reprogrammed state, we asked what role, if any, did the UPR^{ER} play in the reprogramming process. To address this question, we modulated the UPR^{ER} during reprogramming either pharmacologically or genetically. Pharmacologically, we transiently activated the UPR^{ER}, during periods when the UPR^{ER} is normally activated in many, but not all, cells (described in detail below), using APY29, a drug that activates the ribonuclease activity of IRE1 (fig. S4A) (*23*). Strikingly, the early and transient activation of the UPR^{ER} with APY29 during the period when the UPR^{ER} is normally activated during reprogramming (days 4 to 7) increased the percentage of cells expressing the SSEA-4 and TRA-1-60 markers, the most mature in the reprogramming process (Fig. 3A). To rule out that this could be due to increased rates of cell proliferation, we measured cellular proliferation in our experiments and found that it was not increased (fig. S4B).

Intrigued by the positive and transient pharmacological manipulation of the UPR^{ER} upon reprogramming, we investigated whether genetic overexpression of XBP1s could increase cellular reprogramming efficiency. Consistent with the previous pharmacological results, overexpression of XBP1s increased reprogramming efficiency. This increased efficiency was dependent on the transcriptional activity of XBP1s, since overexpression of a mutant version of XBP1s that lacked the DNA binding domain (XBP1s-DBD) was unable to promote reprogramming (Fig. 3B). Furthermore, we confirmed that the increased reprogramming efficiency was not caused by a higher proliferation rate due to XBP1s overexpression (fig. S4C). Conversely and complementary, knockdown of either XBP1 or ATF4 by multiple, distinct short hairpin RNAs significantly reduced the efficiency of reprogramming (Fig. 3C and fig. S4, D and E). Last, the increased numbers of iPSCs created by the overexpression of XBP1s were pluripotent based on their ability to express pluripotency genes and differentiate into teratomas composed of cells formed from all three germ layers as well as directly differentiate them into cells of the mesodermal and endodermal lineage (Fig. 4 and fig. S5). We were also able to expand these observations by reprogramming primary human fibroblast using an episomal reprogramming approach (fig. S6) (*24*).

Together, UPR^{ER} activation is not only necessary but also sufficient to promote reprogramming of somatic cells to a pluripotent state. On the basis of these results, we conclude that at least one arm of the proteostasis network, the UPR^{ER}, plays a vital role in the cellular reidentification process of cellular reprograming.

Activation of the UPR^{ER} during reprogramming is transient

After isolating iPSC colonies for characterization, we observed that the ability to properly spread and expand iPSC cells was lower when cells overexpressed XBP1s driven by the EF1α promoter with retroviral reprogramming. These colonies remained rounded after isolation, leading to their subsequent loss in culture. On the contrary, using the episomal reprogramming method, successful iPSC clonal derivation was very similar between the GFP control and XBP1s overexpression driven by a cytomegalovirus (CMV) promoter, albeit the XBP1s iPSC colonies were more numerous. The EF1α promoter is rarely silenced in ESCs, contrary to the CMV promoter (*25*). This led us to postulate that sustained high levels of XBP1s in iPSCs, by expression using the EF1α promoter, prevent proper spreading and expansion and that the UPR^{ER} is required only transiently during reprogramming. Furthermore, UPR^{ER} activation could be detrimental to the fully formed iPSC, consistent with our analysis of transient UPR^{ER} activation during reprogramming (Figs. 1C and 3A and fig. S2A). Consistent with this hypothesis, all of the EF1α promoter–driven XBP1s iPSC-derived clones had similar *XBP1s* levels compared to the emGFP iPSC lines, suggesting silencing of the ectopic XBP1s transgene driven by the EF1α promoter (Fig. 5A). In addition, the XBP1s-DBD (coding for the transcriptionally inactive XBP1s) iPSC-derived clones, driven by the same EF1α promoter, did not down-regulate the XBP1s-DBD transgene (Fig. 5A). The XBP1s-DBD transgene does not induce the UPR^{ER}. Consistent with these observations, iPSC-derived clones from emGFP overexpression remained fluorescent. The transgene was only silenced when it led to activation of the UPR^{ER} (XBP1s overexpression). Accordingly, overexpression of XBP1s using the EF1α promoter in H9 ESCs caused abnormal colony morphology with a higher density of cells within the colony with no clear colony edges and a more tridimensional growth pattern (fig. S7A). Notably, basal levels of UPR^{ER} activity were similar, or lower, in ESCs compared with their differentiated counterparts as measured by HSPA5-GFP levels (Fig. 5B) and protein levels of ATF4, ATF6, and HSPA5 (Fig. 5C). These observations are consistent with transcriptome analyses of cellular reprogramming (table S1) (*26*). Furthermore, we observed that cells undergoing cellular reprogramming transiently activated the UPR^{ER}, as analyzed by both mRNA (Fig. 5D) and protein levels (Fig. 1C and fig. S2A). Therefore, activation of the UPR^{ER} must be transient during reprogramming and appears detrimental once the cell achieves pluripotency.

Levels of UPR^{ER} activation positively correlate with the reprogramming efficiency

Because reprogramming efficiency could be increased by the activation of the UPR^{ER} and decreased by the loss of XBP1 or ATF4, we postulated that the ability to ectopically induce the UPR^{ER} of individual, genetically identical, somatic cells cultured in identical conditions could be stochastic and might also outline part of the variable nature of the process of cellular reprogramming. To address this question, we followed the induction of the HSPA5-GFP reporter within individual cells in a population undergoing cellular reprogramming. We found a Gaussian distribution of HSPA5-GFP fluorescence among the cell population undergoing reprogramming (Fig. 6A), indicating that UPR^{ER} activation was variable across the cell population. To test whether the intrinsic ability of a cell to induce the UPR^{ER} was predictive of further success along the reprogramming process, we subdivided the Gaussian-distributed HSPA5-GFP population

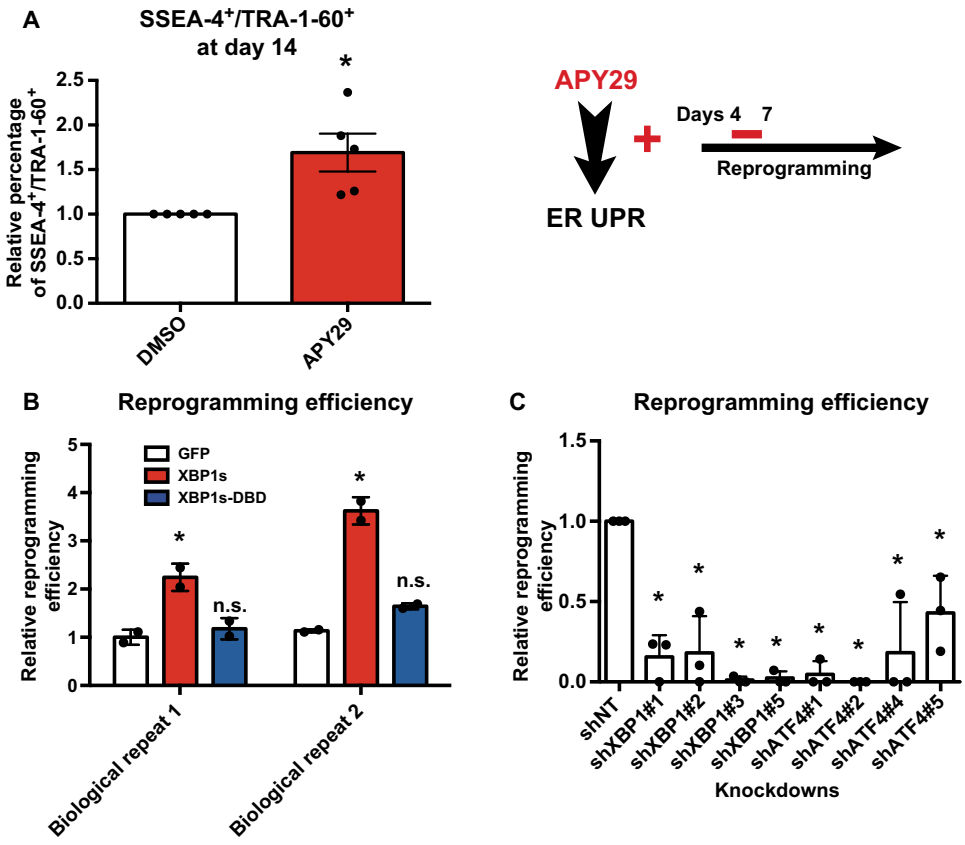

Fig. 3. Ectopic activation of the UPR^{ER} increases the reprogramming efficiency. (**A**) Percentage of SSEA-4$^+$/TRA-1-60$^+$ cells at day 14 of reprogramming after drug treatment with APY29 (0.625 μM), an inducer of the UPR^{ER}, from day 4 to day 7 of reprogramming ($n = 5$, average ± SEM). *$P < 0.05$, statistical significant difference using an unpaired two-tailed t test. (**B**) Relative reprogramming efficiency of keratinocytes measured by colony TRA-1-60 staining after 3 weeks in culture upon overexpression of emGFP, XBP1s, and XBP1s-DBD (missing its DNA binding domain) with the EF1α promoter. Two biological replicates done in duplicate are shown (average ± SD). *$P <$ 0.05, statistical difference using a Dunnett's multiple comparison test to the control. (**C**) Relative reprogramming efficiency of keratinocytes measured by colony TRA-1-60 staining after 3 weeks in culture upon knockdown of XBP1 and ATF4 ($n = 3$, average ± SD). *$P < 0.05$, statistical difference using a Dunnett's multiple comparison test to the control.

at day 8 of reprogramming into three equal subpopulations (low, medium, and high UPR^{ER} induction via GFP levels) (Fig. 6A). We found that the percentage of cells most progressed and more likely to form iPSCs, SSEA-4$^+$/TRA-1-60$^+$ cells, was highest in cells with the highest levels of HSPA5-GFP (Fig. 6A). We expanded this observation to multiple time points during reprogramming and found that we could not break the correlation between UPR^{ER} induction and increased reprogramming efficiency (Fig. 6B).

To further interrogate the predictive value of the UPR^{ER} induction and iPSC formation, we sorted cells at day 7 of reprogramming based on their levels of HSPA5-GFP into two populations, high and low levels (fig. S7B), and assessed iPSC colony formation. After 10 days in culture, cell colonies were stained for TRA-1-60. As predicted, cells with higher levels of HSPA5-GFP at day 7 gave rise to more iPSC colonies (Fig. 6C). We next tested if the reprogramming process was faster in cells with higher levels of UPR^{ER} induction. We reasoned that if this was the case, then the size of the colonies would be larger compared with cells with low UPR^{ER} induction. We measured the area of the iPSC colonies from Fig. 6C, and there were no significant differences in size of the colonies, suggesting that cells with higher UPR^{ER} induction do not reprogram faster (Fig. 6D). These finding indicate that the intrinsic ability of a somatic cell to induce the UPR^{ER} is predictive of its likelihood of becoming pluripotent.

Because c-MYC is a proto-oncogene that facilitates genomic instability and its ectopic overexpression could lead to deleterious side effects during transplantation of iPSCs into hosts, we asked if we could bypass the need for c-MYC using the intrinsic induction of the UPR^{ER} in combination with three of the four reprogramming factors, OCT4, SOX2, and KLF4 (3F). We found high levels of UPR^{ER} induction in cells that had progressed the furthest in the reprogramming process using only three factors (SSEA-4$^+$/TRA-1-60$^+$), consistent with our analysis with all four factors (fig. S8A). In addition, higher HSPA5-GFP correlated with increased percentage of SSEA-4$^+$/TRA-1-60$^+$ cells (fig. S8B). Consistent with this observation, cells with higher levels of HSPA5-GFP at day 7 gave rise to more iPSC colonies (fig. S8C), indicating that induction of the UPR^{ER} could be used as an alternative approach to circumvent potential off-target side effects that might be negative when creating iPSCs with potential pro-oncogenes. Strikingly, the early and transient activation of the UPR^{ER} with APY29 during reprogramming with three factors (days 4 to 7) increased the percentage of cells expressing the SSEA-4 and TRA-1-60 markers, the most mature in the reprogramming process (fig. S8D).

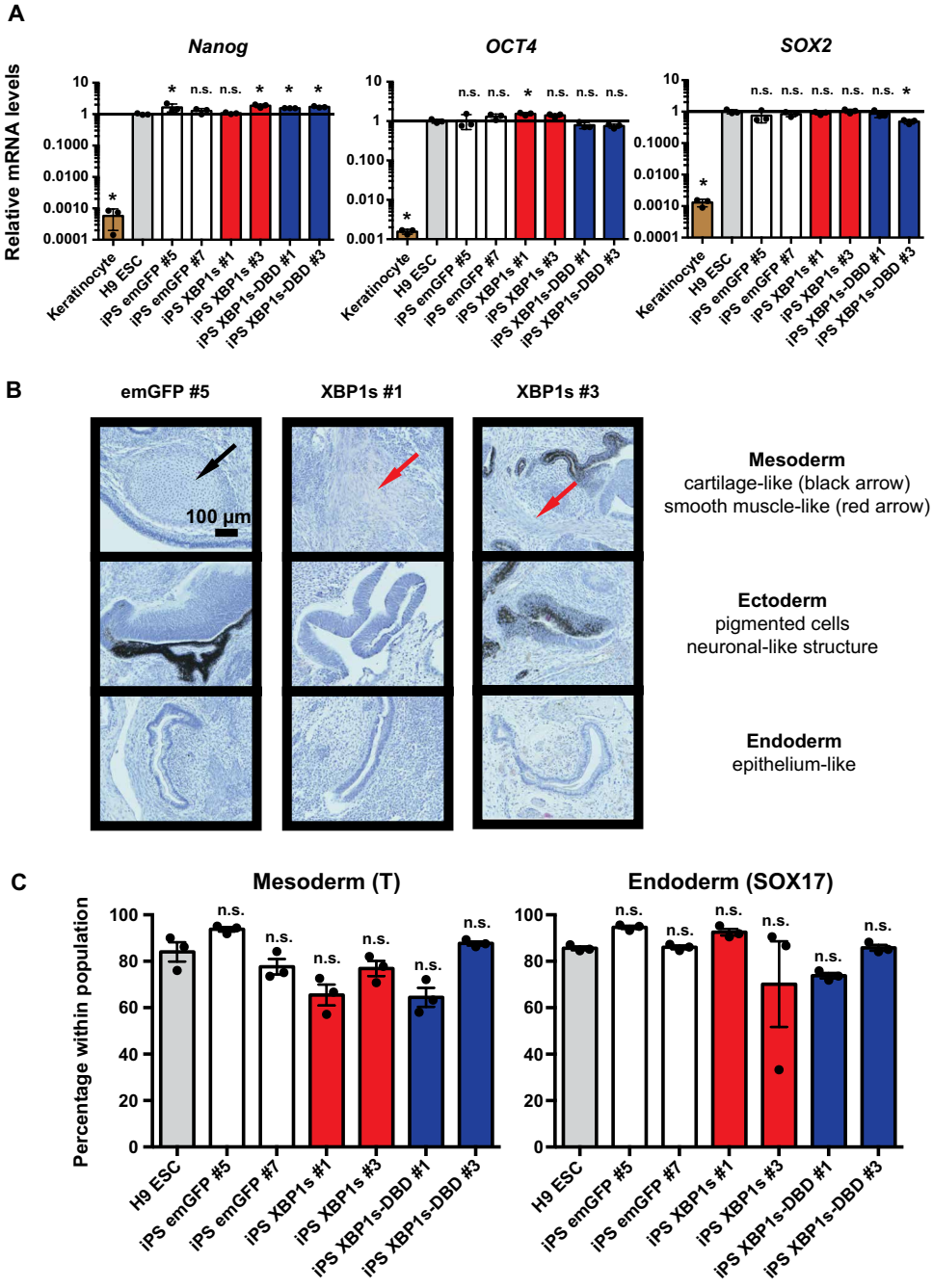

Fig. 4. Derived iPSCs express their endogenous pluripotent genes and are pluripotent. (**A**) Relative endogenous mRNA levels of pluripotent genes in the derived iPSC lines relative to *GAPDH* determined by qRT-PCR ($n = 3$, average ± SD). Values for H9 ESCs were set to 1. *$P < 0.05$, statistical difference using a Dunnett's multiple comparison test to the control H9 ESC. (**B**) Hematoxylin and eosin staining of teratomas showing the three germ layers: mesoderm, ectoderm, and endoderm. Teratoma formation assays were performed after confirmation of the exogenous XBP1s silencing (see Fig. 5A). (**C**) Directed lineage-specific differentiation efficiencies assed by the percentage of cells expressing Brachyury (T) for mesoderm and SOX17 for endoderm differentiation by flow cytometry ($n = 3$, average ± SEM). n.s. indicates nonstatistical difference ($P < 0.05$) using a Dunnett's multiple comparison test to the control H9 ESC.

DISCUSSION

The details and mechanics required for successful cellular reprogramming are becoming more apparent, but the factors responsible for its low efficiency are more difficult to determine, due to the stochastic nature of the process (*3*). The extremely low efficiency can be augmented by the addition of supplementary factors such as other pluripotency-associated factors, cell cycle–regulating genes, and epigenetic modifiers (*4*). However, none of these factors address the role of the proteostasis network or organelle integrity as an important driver for reprogramming. We find that early ER stress is

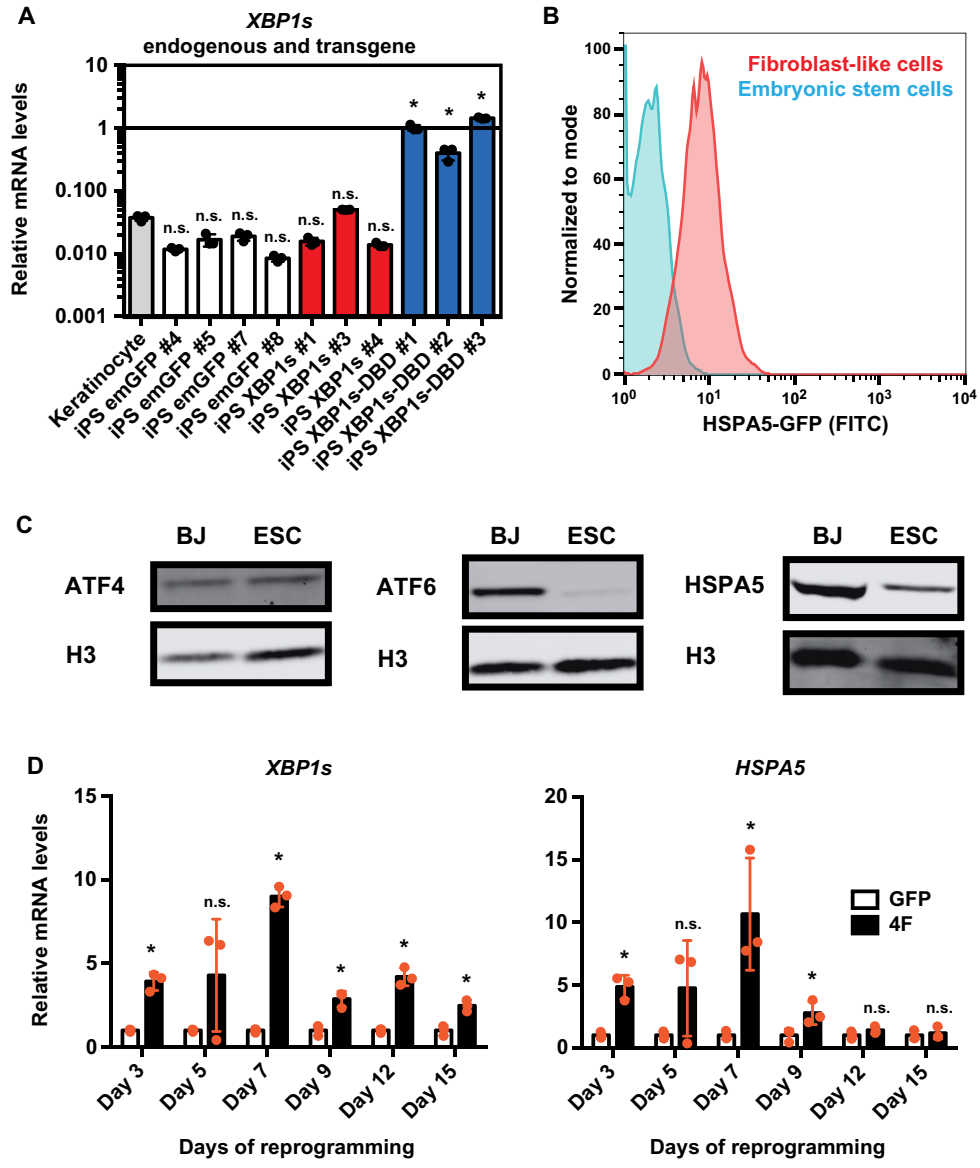

Fig. 5. Transient activation of the UPR^{ER} is necessary during reprogramming. (**A**) Relative mRNA levels of *XBP1s* relative to *GAPDH* determined by qRT-PCR in iPSC colonies derived from either *emGFP*, *XBP1s*, or *XBP1s-DBD* driven by the EF1α promoter ($n = 3$, average ± SD). NB: This primer set will also recognize the *XBP1s-DBD* form. *$P < 0.05$, statistical difference using a Dunnett's multiple comparison test to the control keratinoytes. (**B**) Flow cytometry analysis of HSPA5-GFP in ESC HSPA5-GFP and the differentiated fibroblast-like cells. FITC, fluorescein isothiocyanate. (**C**) Western blot analysis of ATF4, ATF6, and XBP1 in pluripotent stem cells and fibroblasts. Equal number of cells was loaded. (**D**) Relative mRNA levels of *XBP1s* and *HSPA5* relative to *GAPDH* determined by qRT-PCR during the course of cellular reprogramming ($n = 3$, average ± SD). GFP control was set to 1 for each day. *$P < 0.05$, statistical significant difference using an unpaired two-tailed *t*-test.

an essential step for a somatic cell to reprogram and that ectopic transient activation of the UPR^{ER} increases reprogramming efficiency. Moreover, the stochastic nature of the reprogramming process could be partially explained by the ability of a cell to properly mount an ER stress response and can be used as a predictive marker of successful reprogramming (Fig. 6E).

We were surprised that XBP1s can robustly increase reprogramming efficiency, and its requirement was not previously observed in reprogramming paradigms. One explanation could be that XBP1s is transiently up-regulated during reprogramming. In addition, XBP1 activation requires a regulatory splicing event, while most of the other reprogramming factors were inferred on the basis of their high levels in the ESCs. Strikingly, the transient activation of the UPR^{ER} during the early phase of reprogramming using the IRE1 activating drug, APY29, was sufficient to increase its efficiency.

XBP1s, among other UPR^{ER} effectors, is required during development and differentiation (*14*). Thus, consistent with the original hypothesis to identify reprogramming factors using genes required for normal development and differentiation could help reprogram better by enabling a successful transition between the two cell states. Therefore, it is intriguing that a central player of the proteostasis network plays an essential role not only in development but also in reprogramming.

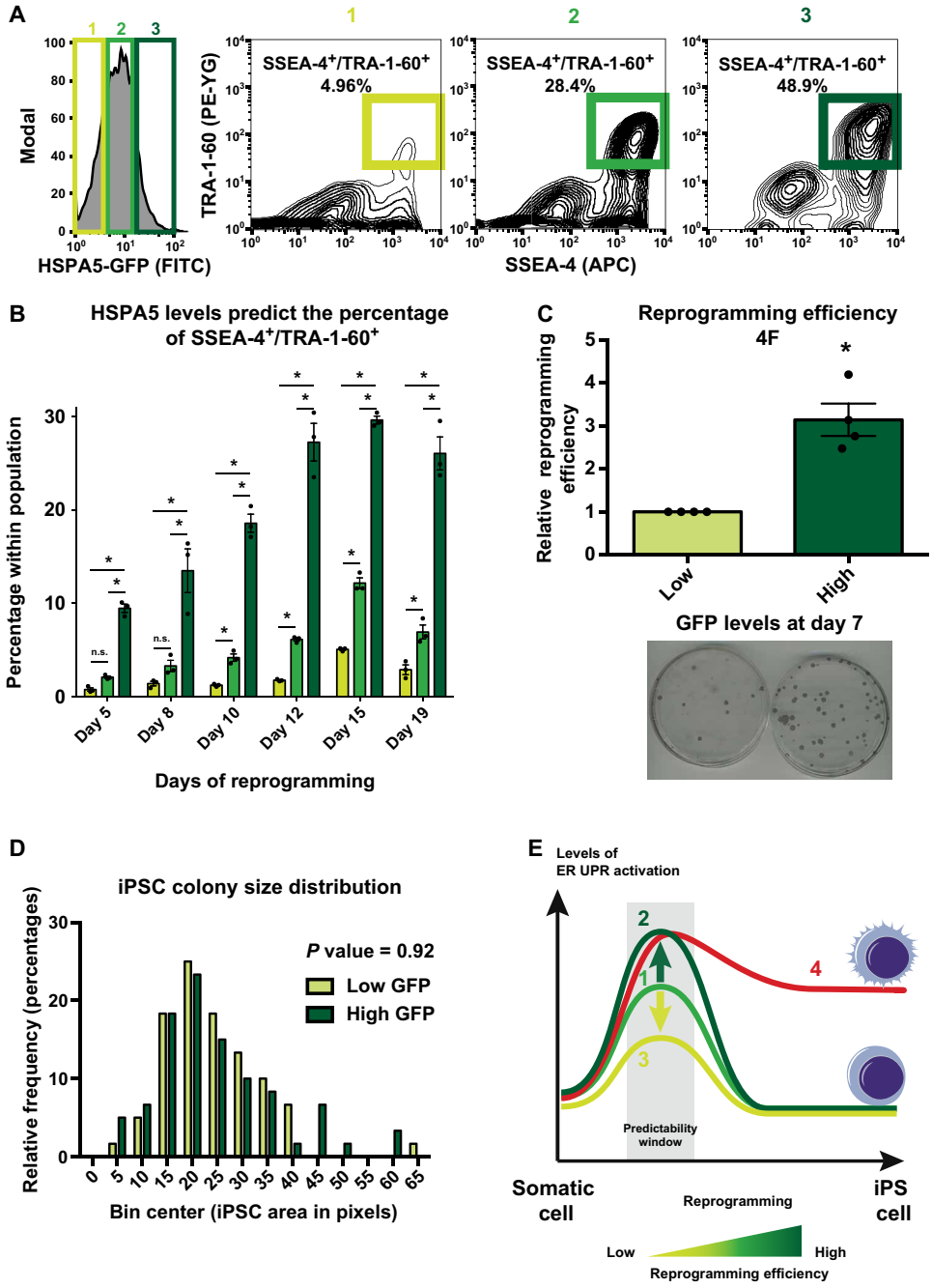

Fig. 6. HSPA5-GFP levels predict the reprogramming efficiency. (**A**) Histogram of fibroblast-like HSPA5-GFP at day 8 of reprogramming. 1, 2, and 3 subdivide the population into three equal parts. Each of them is represented in the right panel by their SSEA-4 and TRA-1-60 staining. The percentage of double positive cells within each of these populations is shown. (**B**) Percentage of SSEA-4$^+$/TRA-1-60$^+$ cells within each population 1, 2, and 3 during reprogramming ($n = 3$, average ± SD). *$P < 0.05$, statistical difference using Newman-Keuls multiple comparison test between all the conditions for each day. (**C**) Upper panel shows relative reprogramming efficiency of fibroblast-like HSPA5-GFP sorted at day 7 of reprogramming based on their GFP levels and assessed by TRA-1-60 colony staining ($n = 4$, average ± SEM). Lower panel shows a representative picture of the staining. *$P < 0.05$, statistical difference using an unpaired two-tailed t test. (**D**) iPSC colony size distribution from the experiment in (C). The area of ~60 iPSC colonies was measured with ImageJ. There was no significant difference in the mean colony size (unpaired two-tailed t test). (**E**) Cells undergoing a successful cellular reprogramming activate the UPR^{ER} transiently (1). Increased levels of UPR^{ER} activation increase the efficiency of cellular reprogramming, (2) while decreasing the UPR^{ER} activation negatively affects the efficiency of cellular reprogramming (3). In our experimental design, it is possible to predict the efficiency of reprogramming based on the levels of UPR^{ER} activation around day 7, depicted by the predictability window. Cells unable to decrease the levels of UPR^{ER} activation give rise to iPSCs unable to properly spread (4).

The mechanism through which the activation of the UPR^{ER} increases reprogramming efficiency remains to be elucidated. The UPR^{ER} activation leads to a global reduction in protein synthesis (*10*) and the degradation of mRNA associated with the ER membrane (*27*). One possibility is that the ER proteome is cleared from a substantial part of its somatic signature, allowing the new pluripotent proteome to be set. Therefore, the activation of the UPR^{ER} must be transient, which is supported by our findings. In addition, the ectopic activation of the UPR^{ER} could provide a cytoprotective buffer to explore different states and consequently reach pluripotency without inducing apoptosis during the reprogramming process. Consistent with this idea, cells with a higher level of UPR^{ER} activation reprogram at a higher rate. Although less explored, bidirectional regulation between DNA damage responses and the UPR^{ER} has been shown (*28*). A cluster of DNA damage and DNA repair genes was identified as a direct target of XBP1s (*29*). Although not explored here, this could allow the potential to counter the negative effects of c-MYC, a well-known inducer of genomic instability, without affecting negatively the reprogramming efficiency as supported by our data. While three-factor reprogramming had increased efficiency when the UPR^{ER} was activated, we question whether replacing c-MYC with XBP1s would meet the needs of the field, as three-factor reprogramming is extremely inefficient. Instead, induction of UPR^{ER} with a transient drug, such as APY29, in combination with the four Yamanaka factors may prove extremely useful for clinical applications and for cells difficult to reprogram.

We predict that effectors ensuring protein quality control can be potent facilitators of reprogramming in assisting the transition from one cell state to another. Previous work in our laboratory (*30*) and others (*31*) has already linked protein quality control through the ubiquitin-proteasome system with stem cell maintenance, differentiation, and reprogramming. The role of other regulatory elements of protein quality control, such as the UPR^{mt}, and molecular chaperones involved in the HSR remain largely unexplored in the regulation of stem cell differentiation or reprogramming. How these processes are involved in reprogramming, as well as their potential cross-play with the UPR^{ER}, will need to be explored. We believe that our observations could also be relevant to transdifferentiation paradigms.

MATERIALS AND METHODS

Cell culture

Human dermal fibroblasts (Lonza, CC-2511 and CC-2509), HEK293FT (Thermo Fisher Scientific, R70007), BJ human fibroblasts (American Type Culture Collection, CRL-2522), fibroblast-like cells, and irradiated CF-1 mouse embryonic fibroblasts (GlobalStem) were grown in Dulbecco's modified Eagle's medium (DMEM), 10% fetal bovine serum (FBS), 1× penicillin/streptomycin (pen/strep), 1× glutamax, and 1× nonessential amino acids (NEAAs) (all from Invitrogen).

The human ESC line H9 (WA09, WiCell Research Institute) and the other human iPS generated lines were cultured with mTeSR1 media (STEMCELL Technologies) on Geltrex (Invitrogen). Human keratinocytes (Lonza, 192907) were cultured with KGM-Gold media (Lonza).

Plasmids

A list of the plasmids and the cloning strategy can be found in table S2.

Viral production

Lentiviral- and moloney-based retroviral pMX-derived vectors were cotransfected with their respective packaging vectors in HEK293FT cells using jetPRIME transfection reagent to generate viral particles, as previously described (*18*). The viral supernatant was filtered through a 0.45-μm filter.

iPSC generation

Primary cells were spinfected with the viral supernatant containing the reprogramming factors and other factors for 1 hour at 1000*g* in the presence of polybrene (8 μg/ml) (Millipore) twice, 24 hours apart. The regular media was replaced after each round. Selection was started the next day of the last transfection; 48 hours later, cells were dissociated with TrypLE (Invitrogen) and plated on top of irradiated mouse embryonic fibroblasts (MEFs) in their regular media. The next day, cells were switched to iPS media containing DMEM/F12, 20% knockout serum replacement, 1× pen/strep, 1× glutamax, 1× NEAA, basic fibroblast growth factor (10 ng/ml) (all from Invitrogen), and 55 μM β-mercaptoethanol (Sigma-Aldrich). To evaluate the reprogramming efficiency, the number of plated cells was counted; after 2 to 3 weeks, cells were fixed with 4% paraformaldehyde (PFA) and stained for TRA-1-60 as previously described (*32*) and scored. Briefly, fixed cells were blocked for 1 hour at room temperature in 1× phosphate-buffered saline (PBS), 3% FBS, and 0.3% Triton X-100 and then incubated with biotin anti–TRA-1-60 (1:250; eBioscience, 13-8863-82) overnight at 4°C and, the next day, streptavidin horseradish peroxidase (1:500; BioLegend, 405210) for 2 hours at room temperature. Staining was developed with the SigmaFast DAB Kit (D0426). Alternatively, an alkaline phosphatase (AP) staining was performed for episomal reprogramming experiments as instructed by the Millipore Detection Kit (SCR004). Briefly, cells were fixed in 4% PFA for less than a minute to avoid losing the AP activity. Cells were rinsed with TBS-T (tris-buffered saline-Tween20) and covered with fast red violet solution/water/naphthol (2:1:1) for 20 min, followed by a wash with PBS. AP-positive colonies were then counted.

For time course studies, imaging, and flow cytometry, cells were plated on Geltrex-coated plates instead of MEFs. Where indicated, after plating on Geltrex, cells were incubated with APY29 (ChemScene, CS-2552) for 3 days.

Alternatively, cells were also reprogrammed using an episomal electroporation system (*24*). Briefly, cells were first selected with the appropriate factor. A total of 500,000 cells were then electroporated with the episomal constructs using the Nucleofector Kit (Lonza, VPD-1001). Cells were plated and kept in their original media. After 6 days, cells were dissociated and plated on freshly plated MEFs. Cells were switched to iPS media the next day.

Derivation of fibroblast-like cells

Stem cells were differentiated into fibroblast-like cells using an embryoid body (EB)–mediated protocol. Stem cells grown on Geltrex were detached using dispase; resuspended in DMEM/F12, 20% FBS, 1× glutamax, 1× NEAA, 1× pen/strep, and 55 μM β-mercaptoethanol; and grew on low-adhesion plates for 4 days with media change. EBs were plated on gelatin-coated plates and cultured with the same media. When EBs spread and cells appeared fibroblast looking, the culture was dissociated using TrypLE and replated using a regular fibroblast media. This was serially done until the whole population became uniform.

RNA isolation and real-time PCR

Cells were collected in TRIzol. A classic chloroform extraction followed by a 70% ethanol precipitation was performed. The mixture was then processed through column using the RNeasy Qiagen Kit,

as described by the manufacturer. The QuantiTect Reverse Transcription Kit (Qiagen) was used to synthesize complementary DNA. Real-time PCR was performed using SYBR Select Mix (Life Technologies). *GAPDH* expression was used to normalize gene expression values. Primer sequences can be found in table S2.

Western blot analysis

Cells were washed with PBS, and radioimmunoprecipitation assay (RIPA) buffer was added to the plates on ice. Cells were scraped, collected, and stored at −20°C. The RIPA buffer was always supplemented with Roche cOmplete mini and phosSTOP when needed. Protein (20 μg) was loaded per lane, and actin or histone H3 was used as a loading control in precast 4 to 12% bis-tris NuPAGE gels (Invitrogen). Proteins were blotted on nitrocellulose membranes using the NuPAGE reagents according to the manufacturer's instructions. Membranes were prepared for imaging using Odyssey CLx Imaging System LI-COR Biosciences with the appropriate reagents. Briefly, membranes were incubated in the proprietary blocking buffer for 1 hour at room temperature. Overnight primary antibody incubation at 4°C was done using the blocking buffer and 0.1% Tween 20. Membranes were washed in TBS-T and then incubated with secondary antibody for 1 hour at room temperature. Membranes were then washed in TBS-T with a final wash in TBS. The software ImageStudio was used to quantify the band intensities. For the list of antibodies and concentrations, refer to table S2.

Fluorescence immunostaining

Cells on slides were fixed with 4% PFA for 15 min and washed with PBS. A 2% donkey serum blocking buffer in PBS was used for 1 hour at room temperature. Primary antibody incubation was done overnight. After PBS washes, secondary antibody was added for 1 hour at room temperature. After PBS washes, slides were mounted with mounting media containing DAPI (4′,6-diamidino-2-phenylindole). For the list of antibodies and concentrations, refer to table S2.

Flow cytometry

For cell analysis, cells were dissociated with TrypLE and pelleted. A 100-μl fluorescent-conjugated antibodies cocktail (5 μl of SSEA-4 330408 and 5 μl of TRA-1-60 330610; BioLegend) in staining media (1× PBS and 2% FBS) was used to resuspend the pellet and incubated 30 min on ice. Cells were then resuspended in excess of staining media, span down and resuspended in staining media, filtered through a cell strainer, and kept on ice. Cells were analyzed using the BD Biosciences LSR Fortessa. The analysis was done using the FlowJo software. For directed mesodermal and endodermal differentiation experiments, a similar workflow was used with the exceptions of using accutase to dissociate the cells and using saponin buffer [saponinin PBS (1 mg/ml) + 1% BSA (bovine serum albumin)] to permeabilize the cells before incubating with fluorescent-conjugated SOX17 (BD Biosciences, 562594) or brachyury (Fisher Scientific, IC2085P) in saponin buffer.

For cell sorting, a similar procedure was followed. Cells were eventually resuspended in their media supplemented with rock inhibitor and sorted accordingly using the BD Biosciences InFlux sorter (fig. S7B). Cells were then transferred to appropriate dishes for culture and kept on rock inhibitor during the next 24 hours.

ER secretion assay

Transduced cells with Gluc–CFP (cyan fluorescent protein) were incubated for 24 hours with fresh media, and the supernatant was collected for analysis. An equal volume of Gluc GLOW buffer (NanoLight Technology) was added to the supernatant in a 96-well plate format. The luminescence was measured by a TECAN plate reader and integrated over 50 ms.

Cell assay

Cells were plated on 96-well plates and treated with the appropriate condition. After the desired incubation time, cell titer glow buffer (Promega) was added to the wells (1:5 volume) and incubated for 12 min on a shaker. The luminescence was measured with the TECAN plate reader and integrated over 1 s.

Electron microscopy

Cells were fixed with 2% glutaraldehyde in 0.1 M phosphate buffer for 5 min. Samples were rinsed with 0 .1 M sodium cacodylate buffer (3× 5 min each), followed by the addition of 1% osmium tetroxide and 1.5% ferrocyanide in 0.1 M cacodylate buffer (5 min). After washing with water (3× 5 min each), 2% uranyl acetate was added for 5 min, followed by a water rinse. A dehydration series of ethanol was then completed: 35, 50, 75, 100, and 100% (5 min each). A 1:1 ethanol/resin (3× 10 min each) incubation followed by 100% resin (3× 10 min each) was done. The samples were cured over 48 hours and then sectioned at 50 nm with a microtome using a Diatome. Sections were placed on a coated copper mesh grid. They were then stained with uranyl acetate for 5 min and then stained with lead citrate for 5 min before imaging.

Genome editing and Southern blot analysis

TALENs technology was used to create an HSPA5-GFP fusion by insertion of eGFP-PGK-Puro at the 3′ end of the HSPA5 locus. We followed the protocol described in (*33*). TALENs were cloned to bind ACAGCAGAAAAAGATGA and ATTACAGCACTAGCA sequences and to generate a double-stranded break proximal to the STOP codon. The donor plasmid OCT4-eGFP-PGK-Puro, published in (*33*), was adapted to target HSPA5 by changing the homology arms. H9 cells were electroporated, and clonal expansion after puromycin selection was done. Successful targeting was confirmed by Southern blot using the GFP probe published in (*33*). Further information can be found in fig. S3A.

Teratoma assay and directed differentiation

Teratoma formation assays were performed as previously described in (*21*). For directed endoderm and mesoderm differentiation, we used STEMdiff kits from STEMCELL Technologies and followed their instructions (catalog nos. 05232 and 05233).

Statistical analysis

The software Excel and Prism were used to perform the statistical tests. The corresponding statistical tests and the number of biological repeats, denoted as *n*, are indicated in the figure legends. When comparing only two conditions, we used a *t* test. If multiple comparisons were done, we corrected for the multiple comparisons. For example, if all the conditions were compared to the control only and no other comparisons between the conditions were intended (e.g., A with B, A with C), then a Dunnett's multiple comparison test was used. If all the conditions were compared to each other (e.g., A with B, B with C, and A with C), then a Newman-Keuls multiple comparison test was used. SD and SEM stand, respectively, for standard deviation and standard error of the mean. For drug dose response assays, a log(drug) versus normalized response with viable slope model was used to determine the EC_{50} (median effective concentration).

SUPPLEMENTARY MATERIALS

Supplementary material for this article is available at http://advances.sciencemag.org/cgi/content/full/5/4/eaaw0025/DC1

Fig. S1. The reprogramming factors activate the three major unfolded protein responses during reprogramming.
Fig. S2. The reprogramming factors activate all the three branches of the UPR^{ER} during reprogramming.
Fig. S3. Activation of the UPR^{ER} and reactivation of the endogenous pluripotent genes during the different cellular reprogramming stages using fibroblast-like HSPA5-GFP cells.
Fig. S4. Modulation of the UPR^{ER} and its impact on cell proliferation.
Fig. S5. Derived iPSCs stain positive for pluripotent genes.
Fig. S6. Episomal reprogramming of fibroblasts by XBP1s overexpression.
Fig. S7. Activation of the UPR^{ER} in stem cells prevents their proper spreading and cell sorting strategy.
Fig. S8. Levels of UPR^{ER} activation are predictive of the reprogramming efficiency using 3F.
Table S1. Transcriptome analysis of UPR^{ER} genes in fibroblasts, iPSCs, and ESCs.
Table S2. List of reagents used.
References (*34*–*36*)

REFERENCES AND NOTES

1. J. M. Polo, E. Anderssen, R. M. Walsh, B. A. Schwarz, C. M. Nefzger, S. M. Lim, M. Borkent, E. Apostolou, S. Alaei, J. Cloutier, O. Bar-Nur, S. Cheloufi, M. Stadtfeld, M. E. Figueroa, D. Robinton, S. Natesan, A. Melnick, J. Zhu, S. Ramaswamy, K. Hochedlinger, A molecular roadmap of reprogramming somatic cells into iPS cells. *Cell* **151**, 1617–1632 (2012).
2. K. Takahashi, S. Yamanaka, Induction of pluripotent stem cells from mouse embryonic and adult fibroblast cultures by defined factors. *Cell* **126**, 663–676 (2006).
3. Y. Buganim, D. A. Faddah, R. Jaenisch, Mechanisms and models of somatic cell reprogramming. *Nat. Rev. Genet.* **14**, 427–439 (2013).
4. K. Takahashi, S. Yamanaka, A decade of transcription factor-mediated reprogramming to pluripotency. *Nat. Rev. Mol. Cell Biol.* **17**, 183–193 (2016).
5. T. Vierbuchen, M. Wernig, Molecular roadblocks for cellular reprogramming. *Mol. Cell* **47**, 827–838 (2012).
6. D. Vilchez, M. S. Simic, A. Dillin, Proteostasis and aging of stem cells. *Trends Cell Biol.* **24**, 161–170 (2014).
7. P. Walter, D. Ron, The unfolded protein response: From stress pathway to homeostatic regulation. *Science* **334**, 1081–1086 (2011).
8. M. Calfon, H. Zeng, F. Urano, J. H. Till, S. R. Hubbard, H. P. Harding, S. G. Clark, D. Ron, IRE1 couples endoplasmic reticulum load to secretory capacity by processing the *XBP-1* mRNA. *Nature* **415**, 92–96 (2002).
9. H. Yoshida, T. Matsui, A. Yamamoto, T. Okada, K. Mori, XBP1 mRNA is induced by ATF6 and spliced by IRE1 in response to ER stress to produce a highly active transcription factor. *Cell* **107**, 881–891 (2001).
10. H. P. Harding, Y. Zhang, D. Ron, Protein translation and folding are coupled by an endoplasmic-reticulum-resident kinase. *Nature* **397**, 271–274 (1999).
11. K. M. Vattem, R. C. Wek, Reinitiation involving upstream ORFs regulates *ATF4* mRNA translation in mammalian cells. *Proc. Natl. Acad. Sci. U.S.A.* **101**, 11269–11274 (2004).
12. K. Haze, H. Yoshida, H. Yanagi, T. Yura, K. Mori, Mammalian transcription factor ATF6 is synthesized as a transmembrane protein and activated by proteolysis in response to endoplasmic reticulum stress. *Mol. Biol. Cell* **10**, 3787–3799 (1999).
13. Y. Wu, Y. Li, H. Zhang, Y. Huang, P. Zhao, Y. Tang, X. Qiu, Y. Ying, W. Li, S. Ni, M. Zhang, L. Liu, Y. Xu, Q. Zhuang, Z. Luo, C. Benda, H. Song, B. Liu, L. Lai, X. Liu, H.-F. Tse, X. Bao, W.-Y. Chan, M. A. Esteban, B. Qin, D. Pei, Autophagy and mTORC1 regulate the stochastic phase of somatic cell reprogramming. *Nat. Cell Biol.* **17**, 715–725 (2015).
14. K. Kratochvílová, L. Moráň, S. Paďourová, S. Stejskal, L. Tesařová, P. Šimara, A. Hampl, I. Koutná, P. Vaňhara, The role of the endoplasmic reticulum stress in stemness, pluripotency and development. *Eur. J. Cell Biol.* **95**, 115–123 (2016).
15. T. Namba, T. Ishihara, K. Tanaka, T. Hoshino, T. Mizushima, Transcriptional activation of ATF6 by endoplasmic reticulum stressors. *Biochem. Biophys. Res. Commun.* **355**, 543–548 (2007).
16. J. R. Friedman, G. K. Voeltz, The ER in 3D: A multifunctional dynamic membrane network. *Trends Cell Biol.* **21**, 709–717 (2011).
17. C. E. Badr, J. W. Hewett, X. O. Breakefield, B. A. Tannous, A highly sensitive assay for monitoring the secretory pathway and ER stress. *PLOS ONE* **2**, e571 (2007).
18. S. Ruiz, A. D. Panopoulos, N. Montserrat, M.-C. Multon, A. Daury, C. Rocher, E. Spanakis, E. M. Batchelder, C. Orsini, J.-F. Deleuze, J. C. Izpisua Belmonte, Generation of a drug-inducible reporter system to study cell reprogramming in human cells. *J. Biol. Chem.* **287**, 40767–40778 (2012).
19. T. Brambrink, R. Foreman, G. G. Welstead, C. J. Lengner, M. Wernig, H. Suh, R. Jaenisch, Sequential expression of pluripotency markers during direct reprogramming of mouse somatic cells. *Cell Stem Cell* **2**, 151–159 (2008).
20. E. M. Chan, S. Ratanasirintrawoot, I.-H. Park, P. D. Manos, Y.-H. Loh, H. Huo, J. D. Miller, O. Hartung, J. Rho, T. A. Ince, G. Q. Daley, T. M. Schlaeger, Live cell imaging distinguishes bona fide human iPS cells from partially reprogrammed cells. *Nat. Biotechnol.* **27**, 1033–1037 (2009).
21. D. Hockemeyer, F. Soldner, E. G. Cook, Q. Gao, M. Mitalipova, R. Jaenisch, A drug-inducible system for direct reprogramming of human somatic cells to pluripotency. *Cell Stem Cell* **3**, 346–353 (2008).
22. T. S. Mikkelsen, J. Hanna, X. Zhang, M. Ku, M. Wernig, P. Schorderet, B. E. Bernstein, R. Jaenisch, E. S. Lander, A. Meissner, Dissecting direct reprogramming through integrative genomic analysis. *Nature* **454**, 49–55 (2008).
23. C. Hetz, E. Chevet, H. P. Harding, Targeting the unfolded protein response in disease. *Nat. Rev. Drug Discov.* **12**, 703–719 (2013).
24. K. Okita, Y. Matsumura, Y. Sato, A. Okada, A. Morizane, S. Okamoto, H. Hong, M. Nakagawa, K. Tanabe, K.-i. Tezuka, T. Shibata, T. Kunisada, M. Takahashi, J. Takahashi, H. Saji, S. Yamanaka, A more efficient method to generate integration-free human iPS cells. *Nat. Methods* **8**, 409–412 (2011).
25. X. Xia, Y. Zhang, C. R. Zieth, S.-C. Zhang, Transgenes Delivered by Lentiviral Vector are Suppressed in Human Embryonic Stem Cells in A Promoter-Dependent Manner. *Stem Cells Dev.* **16**, 167–176 (2007).
26. W. E. Lowry, L. Richter, R. Yachechko, A. D. Pyle, J. Tchieu, R. Sridharan, A. T. Clark, K. Plath, Generation of human induced pluripotent stem cells from dermal fibroblasts. *Proc. Natl. Acad. Sci. U.S.A.* **105**, 2883–2888 (2008).
27. J. Hollien, J. S. Weissman, Decay of endoplasmic reticulum-localized mRNAs during the unfolded protein response. *Science* **313**, 104–107 (2017).
28. E. Chevet, C. Hetz, A. Samali, Endoplasmic reticulum stress–activated cell reprogramming in oncogenesis. *Cancer Discov.* **5**, 586–597 (2015).
29. D. Acosta-Alvear, Y. Zhou, A. Blais, M. Tsikitis, N. H. Lents, C. Arias, C. J. Lennon, Y. Kluger, B. D. Dynlacht, XBP1 controls diverse cell type- and condition-specific transcriptional regulatory networks. *Mol. Cell* **27**, 53–66 (2007).
30. D. Vilchez, L. Boyer, I. Morantte, M. Lutz, C. Merkwirth, D. Joyce, B. Spencer, L. Page, E. Masliah, W. T. Berggren, F. H. Gage, A. Dillin, Increased proteasome activity in human embryonic stem cells is regulated by PSMD11. *Nature* **489**, 304–308 (2012).
31. S. M. Buckley, B. Aranda-Orgilles, A. Strikoudis, E. Apostolou, E. Loizou, K. Moran-Crusio, C. L. Farnsworth, A. A. Koller, R. Dasgupta, J. C. Silva, M. Stadtfeld, K. Hochedlinger, E. I. Chen, I. Aifantis, Regulation of Pluripotency and Cellular Reprogramming by the Ubiquitin-Proteasome System. *Cell Stem Cell* **11**, 783–798 (2012).
32. T. T. Onder, N. Kara, A. Cherry, A. U. Sinha, N. Zhu, K. M. Bernt, P. Cahan, B. O. Marcarci, J. Unternaehrer, P. B. Gupta, E. S. Lander, S. A. Armstrong, G. Q. Daley, Chromatin-modifying enzymes as modulators of reprogramming. *Nature* **483**, 598–602 (2012).
33. D. Hockemeyer, H. Wang, S. Kiani, C. S. Lai, Q. Gao, J. P. Cassady, G. J. Cost, L. Zhang, Y. Santiago, J. C. Miller, B. Zeitler, J. M. Cherone, X. Meng, S. J. Hinkley, E. J. Rebar, P. D. Gregory, F. D. Urnov, R. Jaenisch, Genetic engineering of human pluripotent cells using TALE nucleases. *Nat. Biotechnol.* **29**, 731–734 (2011).
34. H.-E. Kim, A. R. Grant, M. S. Simic, R. A. Kohnz, D. K. Nomura, J. Durieux, C. E. Riera, M. Sanchez, E. Kapernick, S. Wolff, A. Dillin, Lipid biosynthesis coordinates a mitochondrial-to-cytosolic stress response. *Cell* **166**, 1539–1552.e16 (2016).
35. A. Soufi, G. Donahue, K. S. Zaret, Facilitators and impediments of the pluripotency reprogramming factors' initial engagement with the genome. *Cell* **151**, 994–1004 (2012).
36. S. Ruiz, A. Gore, Z. Li, A. D. Panopoulos, N. Montserrat, H.-L. Fung, A. Giorgetti, J. Bilic, E. M. Batchelder, H. Zaehres, H. R. Schöler, K. Zhang, J. C. Izpisua Belmonte, Analysis of protein coding mutations in hiPSCs and their possible role during somatic cell reprogramming. *Nat. Commun.* **4**, 1382 (2013).

Acknowledgments

Funding: Funding was provided by HHMI, CIRM (RB5-06974), NIA (R01AG042679), and NIH (R01CA196884) grants. E.A.M. is a fellow of The Jane Coffin Childs Memorial Fund for Medical Research; hence, this investigation has been aided by a grant from The Jane Coffin Childs Memorial Fund for Medical Research. We thank B. Tannous for providing the Gluc-CFP, the Tjian lab for the episomal reprogramming vectors, A. Panopoulos and S. Ruiz for the pMX reprogramming vectors and the reprogramming protocols, and R. Forster, J. Boyle, K. Hennick, B. Webster, and G. Qing for technical help. **Ethics statement:** This study was performed in strict accordance with the recommendations in the *Guide for the Care and Use of Laboratory Animals* of the National Institutes of Health. All of the animals were handled according to approved Institutional Animal Care and Use Committee (IACUC) protocols (R355-0114) of the University of California, Berkeley. **Author contributions:** Conceptualization: M.S.S. and A.D. Methodology: M.S.S., R.T.S., E.A.M., and K.H. Formal analysis: M.S.S. Investigation:

M.S.S. Resources: J.J.H., M.S., F.K.L., K.H., and D.J. Writing (original draft): M.S.S. Writing (review and editing): M.S.S, D.H., and A.D. Visualization: M.S.S. Supervision: A.D. Funding acquisition: D.H. and A.D. **Competing interests:** The authors declare that they have no competing interests. **Data and materials availability:** The Gluc-CFP can be provided by B. Tannous pending scientific review and a completed material transfer agreement. Requests for the Gluc-CFP should be submitted to btannous@hms.harvard.edu. All data needed to evaluate the conclusions in the paper are present in the paper and/or the Supplementary Materials. Additional data related to this paper may be requested from the authors.

Submitted 8 November 2018
Accepted 25 February 2019
Published 10 April 2019
10.1126/sciadv.aaw0025

Citation: M. S. Simic, E. A. Moehle, R. T. Schinzel, F. K. Lorbeer, J. J. Halloran, K. Heydari, M. Sanchez, D. Jullié, D. Hockemeyer, A. Dillin, Transient activation of the UPR^{ER} is an essential step in the acquisition of pluripotency during reprogramming. *Sci. Adv.* **5**, eaaw0025 (2019).